

## Story-wise system identification of actual shear building using ambient vibration data and ARX model

Ayumi Ikeda, Kohei Fujita and Izuru Takewaki\*

*Department of Architecture and Architectural Engineering, Kyoto University,  
Kyotodaigaku-Katsura, Nishikyo-ku, Kyoto 615-8540, Japan*

*(Received April 20, 2014, Revised May 6, 2014, Accepted May 7, 2014)*

**Abstract.** A sophisticated story-wise stiffness identification method for a shear building structure is applied to the case where the shear building is subjected to an actual micro-tremor. While the building responses to earthquake ground motions are necessary in the previous method, it is shown that micro-tremors can be used for identification within the same framework. This enhances the extended usability and practicality of the previously proposed identification method. The difficulty arising in the limit manipulation at zero frequency in the previous method is overcome by introducing an ARX model. The weakness of small SN ratios in the low frequency range is avoided by using the ARX model together with filtering and introducing new constraints on the ARX parameters.

**Keywords:** system identification; story-wise stiffness identification; ambient vibration data; shear building; ARX model

---

### 1. Introduction

A great deal of research interest has been focused recently on system identification of civil, mechanical and aerospace structures in response to the increasing need of enhancement of safety and upgrade of ability of damage detection (or damage diagnosis) of various kinds of structures (Hart and Yao 1977, Beck and Jennings 1980, Hoshiya and Saito 1984, Kozin and Natke 1986, Agbabian *et al.* 1991, Koh *et al.* 1991, Yao and Natke 1994, Hjelmstad *et al.* 1995, Ghanem and Shinozuka 1995, Shinozuka and Ghanem 1995, Masri *et al.* 1996, Doebling *et al.* 1996, Hjelmstad 1996, Housner *et al.* 1997, Bernal and Beck 2004, Lus *et al.* 2004, Nagarajaiah and Basu 2009, Ji *et al.* 2011). In response to such circumstance, a series of international conferences have been held (Housner *et al.* 1994, Kobori *et al.* 1998, Casciati 2002, Johnson and Smyth 2006, Fujino *et al.* 2010). The need of system identification results from the accelerated demand of rapid assessment for material aging issues and for continuing use of buildings after earthquakes. A comprehensive review of system identification and damage detection has been provided in the paper (Nagarajaiah and Basu 2009). It is also well-recognized that system identification plays an important role in reducing gaps between the constructed structural systems and their structural design models (model refinement).

---

\*Corresponding author, Professor, E-mail: [takewaki@archi.kyoto-u.ac.jp](mailto:takewaki@archi.kyoto-u.ac.jp)

From the global viewpoint, there are two kinds of branches, i.e. the modal parameter system identification and the physical parameter system identification. The modal parameter system identification is well-established and various types of research have been conducted and accumulated (for example Hart and Yao 1977, Beck and Jennings 1980, Safak 1989). In the modal parameter system identification, the observations at two places at least are necessary for the natural frequency and damping ratio identification. On the other hand, the observations (or interpolation from fewer observations) at many places are usually required for modal shape identification. This is often a cumbersome task.

In contrast to such modal parameter system identification, the physical parameter system identification has been developed for direct identification of physical parameters (stiffness and damping coefficients). For example, Takewaki and Nakamura (2000, 2005) introduced a method based on the work by Udwadia *et al.* (1978). In that method, a shear building model is used and stiffness and damping coefficients of a specific story are identified directly from the floor accelerations just above and below the specific story. However the method by Takewaki and Nakamura (2000, 2005) has a difficulty resulting from the small signal/noise (SN) ratio in the low frequency range and cannot be applied to ambient vibration data, e.g. micro-tremors, and to high-rise buildings with large aspect ratios. The latter problem has been tackled by Kuwabara *et al.* (2013), Minami *et al.* (2013), Fujita *et al.* (2013) by using a shear-bending model.

Hernandez-Garcia *et al.* (2010a, b) have developed an interesting method of damage detection using a floor-by-floor approach to enhance the efficiency and accuracy of the identification results. Xing and Mita (2012) have devised a time-domain substructure damage identification method for shear buildings by focusing a substructure consisting of one story. Zhang and Johnson (2013a, b) have developed another substructure identification method for shear buildings which considers the noise effect of recorded data on identification accuracy and utilizes an iterative inductive procedure from the top story. Furthermore a combined method of the modal parameter system identification and the physical parameter system identification is also well used (for example Hjelmstad *et al.* 1995, Barroso and Rodriguez 2004). After modal parameters are identified, physical parameters are determined by solving inverse problems. Zhang and Johnson (2012) and Johnson *et al.* (2004) explained a method for reducing the noise effect by using cross correlation functions and cross power spectra of structural responses.

The difficulty arising in the limit manipulation in the method by Takewaki and Nakamura (2000, 2005) has been overcome by introducing an ARX model in the previous paper (Kuwabara *et al.* 2013, Maeda *et al.* 2011). The weakness of a small SN ratio in the low frequency range in the method (2000, 2005) has been avoided by using the ARX model and introducing new constraints on the ARX parameters. Another difficulty due to small vibration levels of micro-tremor is tackled in this paper by introducing a combination of the ARX model, filtering in the frequency domain (low-cut filter) and averaging in the time domain (sequential time-window shift for Fourier transformation and averaging). It is shown that the previously proposed story-wise stiffness identification method is applicable to actual recorded data of an ambient vibration level with the help of this sophisticated combination.

## 2. Governing equations for shear building model

Consider an  $N$ -story shear building model with viscous damping as shown in Fig. 1. Let  $m_j$

and  $k_j$  denote the mass of the  $j$ -th floor and the story stiffness of the  $j$ -th story and let  $c_j$  be the viscous damping coefficient of the  $j$ -th story. Since the formulation in the frequency domain is appropriate in the present formulation, all the governing equations are expressed in the frequency domain. Let  $i$  denote the imaginary unit.

Keeping the relations  $\dot{U}(\omega) = i\omega U(\omega)$ ,  $\ddot{U}(\omega) = -\omega^2 U(\omega)$  in mind, the equations of motion in the frequency domain for this shear building model subjected to the horizontal ground (base) acceleration  $\ddot{u}_g$  may be expressed as

$$(-\omega^2 \mathbf{M} + i\omega \mathbf{C} + \mathbf{K})\mathbf{U}(\omega) = -\mathbf{M}\mathbf{1}\ddot{U}_g(\omega) \quad (1)$$

where  $\mathbf{U}(\omega)$  and  $\ddot{U}_g(\omega)$  are the Fourier transforms of the horizontal displacements  $\mathbf{u}(t) = \{u_j(t)\}$  of floors relative to ground and the ground (base) acceleration  $\ddot{u}_g$ , respectively. The mass, stiffness and damping matrices are defined by

$$\mathbf{M} = \text{diag}(m_1 \ m_2 \ \dots \ m_N) \quad (2a)$$

$$\mathbf{K} = \begin{bmatrix} k_1 + k_2 & -k_2 & & \\ -k_2 & k_2 + k_3 & -k_3 & \\ & & \ddots & \\ & & & -k_N \ k_N \end{bmatrix} \quad (2b)$$

$$\mathbf{C} = \begin{bmatrix} c_1 + c_2 & -c_2 & & \\ -c_2 & c_2 + c_3 & -c_3 & \\ & & \ddots & \\ & & & -c_N \ c_N \end{bmatrix} \quad (2c)$$

The vector  $\mathbf{1}$  in the right-hand side of Eq.(1) denotes  $\mathbf{1} = \{1 \ 1 \ \dots \ 1\}^T$ . Equation (1) can be expressed more compactly as

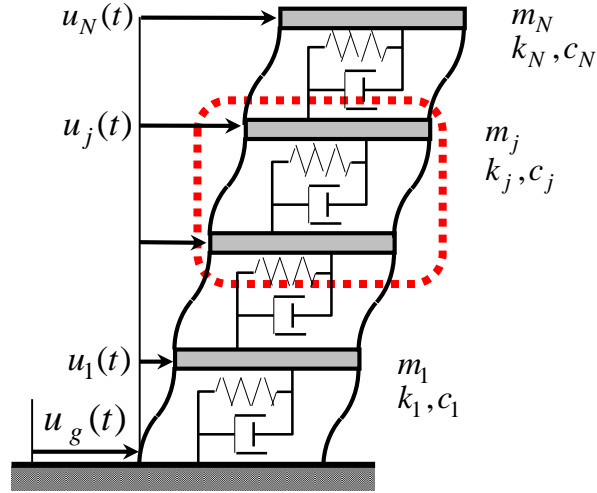
$$\mathbf{A}(\omega)\mathbf{U}(\omega) = -\mathbf{M}\mathbf{1}\ddot{U}_g(\omega) \quad (3)$$

where

$$\mathbf{A}(\omega) = \begin{bmatrix} p_1(\omega) & -q_1(\omega) & & 0 \\ -q_1(\omega) & p_2(\omega) & \ddots & \\ & \ddots & \ddots & -q_{N-1}(\omega) \\ 0 & & -q_{N-1}(\omega) & p_N(\omega) \end{bmatrix} \quad (4)$$

and the frequency-dependent components in  $\mathbf{A}(\omega)$  are defined by

$$\begin{aligned} p_j(\omega) &= -\omega^2 m_j + i\omega c_j + k_j + i\omega c_{j+1} + k_{j+1} \quad (j=1, \dots, N-1) \\ &= -\omega^2 m_j + q_j(\omega) + q_{j+1}(\omega) \end{aligned} \quad (5a)$$

Fig. 1  $N$ -story shear building model with viscous damping

$$\begin{aligned} p_N(\omega) &= -\omega^2 m_N + i\omega c_N + k_N \\ &= -\omega^2 m_N + q_N(\omega) \end{aligned} \quad (5b)$$

$$q_j(\omega) = i\omega c_j + k_j \quad (j=1, \dots, N) \quad (5c)$$

### 3. Stiffness and damping identification

Based on the mathematical formulation (Nakamura and Takewaki 2000), the story stiffness and damping coefficient can be expressed as

$$k_j = \lim_{\omega \rightarrow 0} \left( M_j \times \operatorname{Re} \left[ \frac{(i\omega)^2 (\ddot{U}_g + \ddot{U}_j)}{(\ddot{U}_g + \ddot{U}_{j-1}) - (\ddot{U}_g + \ddot{U}_j)} \right] \right) \quad (6)$$

$$c_j = \lim_{\omega \rightarrow 0} \left( M_j \times \frac{d}{d\omega} \left\{ \operatorname{Im} \left[ \frac{(i\omega)^2 (\ddot{U}_g + \ddot{U}_j)}{(\ddot{U}_g + \ddot{U}_{j-1}) - (\ddot{U}_g + \ddot{U}_j)} \right] \right\} \right) \quad (7)$$

where  $M_j = \sum_{i=j}^N m_i$ . Eq.(6) expresses the modified dynamic equilibrium of the inertial forces above the  $j$ th story with the story shear force in the  $j$ th story. Eqs.(6) and (7) imply that the story stiffness and damping coefficient can be derived only from the accelerations just above and below the object story (see Fig. 2). Eqs. (6) and (7) will be used in the following section.

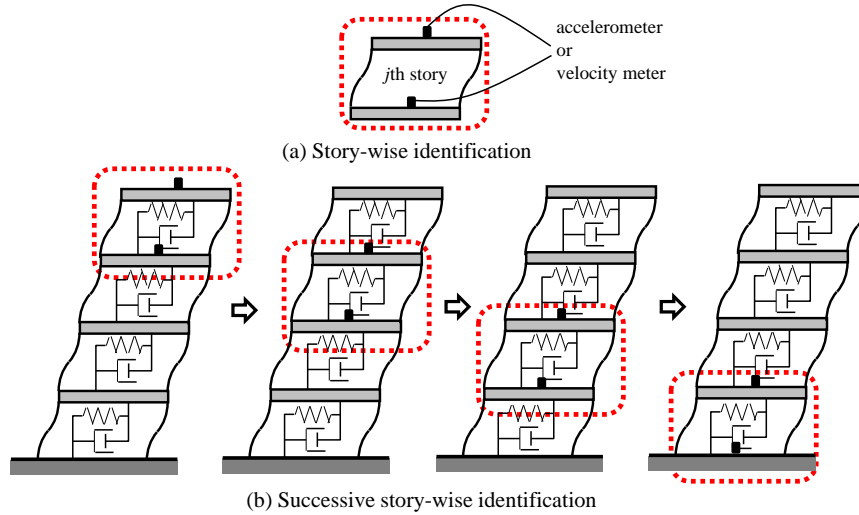


Fig. 2 Sensor location and identification procedure

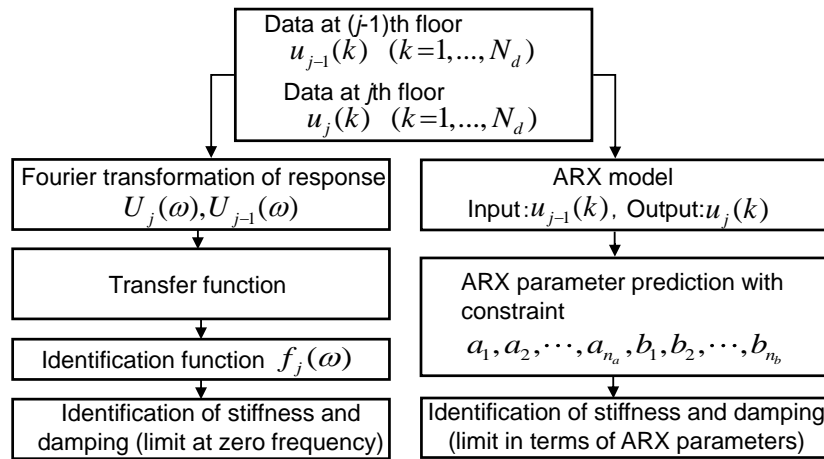


Fig. 3 Original identification method and advanced method using ARX model

#### 4. Identification of stiffness and damping coefficient using ARX model

In the previous method (Nakamura and Takewaki 2000, 2005) for shear building models, the limit manipulation of the identification function  $f_j(\omega)$  for  $\omega \rightarrow 0$  is used. The identification function  $f_j(\omega)$  is defined later in Eq.(10). However, it is often the case that the identification function becomes unstable and exhibits a large variability in the low frequency range. To overcome this difficulty, an ARX model is introduced which is a time-domain model. The reliability of the ARX model in this direction has been confirmed in the papers (Takewaki and Nakamura 2009, Maeda *et al.* 2011). Especially in the paper (Maeda *et al.* 2011), the applicability of the ARX model to shear building models has been demonstrated (see Fig. 3).

#### 4.1 Taylor series expansion of transfer function

Rewrite Eqs.(6) and (7) as follows.

$$k_j = \lim_{\omega \rightarrow 0} \left( \operatorname{Re} [f_j(\omega)] \right) \quad (8)$$

$$c_j = \lim_{\omega \rightarrow 0} \left( \frac{d}{d\omega} \operatorname{Im} [f_j(\omega)] \right) \quad (9)$$

where

$$f_j(\omega) = - \frac{\omega^2 M_j}{\frac{1}{G_{j,j-1}(\omega)} - 1} \quad (10)$$

In Eqs.(8) and (9),  $G_{j,j-1}(\omega)$  is the transfer function between  $j$ th and  $(j-1)$ th floors defined by

$$G_{j,j-1}(\omega) = \frac{\ddot{U}_g + \ddot{U}_j}{\ddot{U}_g + \ddot{U}_{j-1}} \quad (11)$$

This transfer function can also be expressed in terms of the ARX parameters (see Appendix 1).

$$G_{j,j-1}(\omega) = \frac{b_1 e^{-i\omega T_0} + \dots + b_n e^{-in\omega T_0}}{1 + a_1 e^{-i\omega T_0} + \dots + a_n e^{-in\omega T_0}} \quad (12)$$

Consider the Taylor series expansion of  $G_{j,j-1}(\omega)$  as follows.

$$G_{j,j-1}(\omega) \cong A_0 + A_1 \omega + A_2 \omega^2 + \dots \quad (13)$$

From Eqs.(12), (13), the coefficients  $A_0, A_1, A_2, A_3$  of the Taylor series expansion can be expressed in terms of the ARX parameters  $\{a_k\}, \{b_k\}$ .

$$A_0 = \frac{B_n}{C_n} \quad (14a)$$

$$A_1 = i T_0 \frac{B_{1n} C_n - B_n C_{1n}}{C_n^2} \quad (14b)$$

$$A_2 = -\frac{T_0^2}{2} \left[ \frac{B_{2n}}{C_n} - \frac{B_n C_{2n}}{C_n^2} - 2 \frac{B_{1n} C_{1n}}{C_n^2} + 2 \frac{B_n C_{1n}^2}{C_n^3} \right] \quad (14c)$$

$$A_3 = \frac{iT_0^3}{6} \left[ -\frac{B_{3n}}{C_n} + 3\frac{B_{2n}C_{1n}}{C_n^2} + 3\frac{B_{1n}C_{2n}}{C_n^2} + \frac{B_n C_{3n}}{C_n^2} - 6\frac{B_{1n}C_{1n}^2}{C_n^3} - 6\frac{B_n C_{1n}C_{2n}}{C_n^3} + 6\frac{B_n C_{1n}^3}{C_n^4} \right] \quad (14d)$$

where

$$B_n = \sum_{k=1}^n b_k, B_{1n} = \sum_{k=1}^{n-1} (n-k)b_k, B_{2n} = \sum_{k=1}^{n-1} (n-k)^2 b_k, \quad (15)$$

$$B_{3n} = \sum_{k=1}^n b_k \left( n^3 + \sum_{k=1}^{n-1} (n-k)^3 a_k \right)$$

$$C_n = \left( 1 + \sum_{k=1}^n a_k \right), C_{1n} = \left\{ n + \sum_{k=1}^{n-1} (n-k)a_k \right\}, C_{2n} = \left\{ n^2 + \sum_{k=1}^{n-1} (n-k)^2 a_k \right\} \quad (16)$$

$$C_{3n} = \left( n^3 + \sum_{k=1}^{n-1} (n-k)^3 a_k \right)$$

Although examples up to the order ‘three’ have been presented here, higher-order expressions can be obtained if desired.

By introducing the real and imaginary parts of  $A_j$  as

$$A_j = A_j^R + iA_j^I \quad (17)$$

and substituting the properties of the real and imaginary parts of  $A_j$ , the transfer function can be reduced to

$$G_{j,j-1}(\omega) \cong (A_0^R + A_2^R \omega^2 + \dots) + i(A_1^I \omega + A_3^I \omega^3 + \dots) \quad (18)$$

#### 4.2 Relation of the limit value of transfer function with ARX parameters

It is meaningful to note that Eq.(19) can be derived from the mechanical interpretation, i.e. the  $j$ -th floor and  $(j-1)$ -th floor move identically at  $\omega \rightarrow 0$ .

$$\lim_{\omega \rightarrow 0} \operatorname{Re} \{ G_{j,j-1}(\omega) \} = 1 \quad (19)$$

The following relation also holds because  $G_{j,j-1}(\omega)$  should not include linear terms of  $\omega$  judging from Eqs.(8), (9) and (10).

$$\lim_{\omega \rightarrow 0} \frac{d}{d\omega} \operatorname{Im} \{ G_{j,j-1}(\omega) \} = 0 \quad (20)$$

Equation (19) leads to Eq.(21) and Eq.(20) yields Eq.(22).

$$A_0^R = 1 \quad (21)$$

$$A_1^I = 0 \quad (22)$$

Furthermore, the following equations can be derived from Eqs.(14a, b), (21), (22).

$$\sum_{k=1}^n a_k + 1 = \sum_{k=1}^n b_k \quad (23)$$

$$\sum_{k=1}^{n-1} (n-k) b_k \left\{ 1 + \sum_{k=1}^n a_k \right\} = \sum_{k=1}^n b_k \left\{ n + \sum_{k=1}^{n-1} (n-k) a_k \right\} \quad (24)$$

These relations will be used as the constraints in the estimation of the ARX parameters. Eq.(23) is used for stiffness identification and Eq.(24) for damping identification.

#### 4.3 ARX parameter estimation with constraints

The proposed method requires the prediction of the ARX parameters under the conditions on the ARX parameters (Eq.(23) for stiffness identification). It is found that Eq.(23) is a linear equation for the ARX parameters. A batch processing least-squares estimation method (Mendel 1995) (Appendix 2, 3) provides

$$\mathbf{R}\boldsymbol{\theta} = \mathbf{f} \quad (25)$$

By applying the Lagrange multiplier method, the linear constraint can be incorporated into the batch processing least-squares estimation method.

Equation (23) can be expressed by

$$\mathbf{p}^T \boldsymbol{\theta} = -1 \quad (26)$$

where

$$\mathbf{p} = \{1, \dots, 1, -1, \dots, -1\}^T \quad (27)$$

Therefore the present method is reduced to the problem for solving the following equations.

$$\begin{bmatrix} \mathbf{R} & \mathbf{p} \\ \mathbf{p}^T & 0 \end{bmatrix} \begin{Bmatrix} \boldsymbol{\theta} \\ \lambda \end{Bmatrix} = \begin{Bmatrix} \mathbf{f} \\ -1 \end{Bmatrix} \quad (28)$$

#### 4.4 ARX parameter expression of identification function

Substitution of Eq.(21) and (22) into Eq.(18) leads to

$$G_{j,j-1}(\omega) \cong (1 + A_2^R \omega^2 + \dots) + i(A_3^I \omega^3 + \dots) \quad (29)$$

Substitution of Eq.(29) into Eq.(10) and transformation of the denominator into the real number provide

$$\begin{aligned} f_j(\omega) = & \omega^2 M_j \frac{(1 + A_2^R \omega^2 + \dots)(A_2^R \omega^2 + \dots) + (A_3^I \omega^3 + \dots)^2}{(A_2^R \omega^2 + \dots)^2 + (A_3^I \omega^3 + \dots)^2} \\ & + i \omega^2 M_j \frac{(A_2^R \omega^2 + \dots)(A_3^I \omega^3 + \dots) - (1 + A_2^R \omega^2 + \dots)(A_3^I \omega^3 + \dots)}{(A_2^R \omega^2 + \dots)^2 + (A_3^I \omega^3 + \dots)^2} \end{aligned} \quad (30)$$



From Eq. (30), the stiffness can be identified as

$$k_j = \lim_{\omega \rightarrow 0} \{ \operatorname{Re}[f_j(\omega)] \} = \frac{M_j}{A_2^R} \quad (31a)$$

Because  $A_2^R$  is expressed in terms of the ARX parameters as shown in Eq.(14) ( $A_2^R = A_2$  in Eq.(14c)), the stiffness identification problem can be reduced to the estimation problem of the ARX parameters. This means that the proposed method enables one to avoid the setting of approximation functions which is sometimes difficult in the previous method (Takewaki and Nakamura 2000).

Similarly, from Eq. (30), the damping coefficient can be identified as

$$c_j = \lim_{\omega \rightarrow 0} \left( \frac{d}{d\omega} \operatorname{Im}[f_j(\omega)] \right) = -\frac{A_3^I M_j}{(A_2^R)^2} \quad (31b)$$

$A_3^I$  is expressed by  $A_3^I = A_3 / i$  in Eq.(14d). As in the case of stiffness identification, the damping identification problem has been reduced to the estimation problem of the ARX parameters.

## 5. Determination of number of orders of ARX model

It is important to investigate how to determine the number of orders of the ARX model. Let us introduce the following function called ‘Fit’ in the time domain.

$$\text{Fit\_time} = \frac{1}{N_d} \sum_{i=1}^{N_d} \left( \frac{\hat{y}(t_i) - y(t_i)}{\sigma_{raw}} \cdot \frac{y(t_i) - \bar{y}}{\sigma_{raw}} \right)^2 \quad (32)$$

where  $y(t)$  is the recorded output data,  $\sigma_{raw}$  is the standard deviation of  $y$ ,  $\hat{y}(t)$  is the output data computed from the ARX model (Eq.(A9) in Appendix 2) and  $\bar{y}$  is the mean value of  $y(t)$ . It can be said that, if Fit in the time domain is close to 0, the function in terms of the ARX model matches well with the record.

On the other hand, let us introduce another function called ‘Fit’ in the frequency domain.

$$\text{Fit\_frequency} = \frac{\sum_{\omega=\omega_c}^{\omega_{\max}} (\|G\| - \|G_{ARX}\|)^2}{\sum_{\omega=\omega_c}^{\omega_{\max}} (\|G\|)^2} \quad (33)$$

where  $G$  denotes the transfer function computed from the records. Averaging of raw data in time domain (sequential time-window shift for Fourier transformation and averaging) is implemented in this paper for reliable identification. Since the averaging by successive shifting of data window is applied here,  $(\|G\| - \|G_{ARX}\|)^2$  is used.  $\|G - G_{ARX}\|^2$  may not be appropriate in the application of the averaging.  $G_{ARX}$  is the transfer function evaluated by the ARX model.  $\omega_c$  is the cut-off frequency in the high-pass filter (this value will be specified in Section 7) and  $\omega_{\max}$  is specified as

$100 \pi$  (rad/s). It can be said that, if Fit in the frequency domain is close to 0, the function in terms of the ARX model matches well with the record.

## 6. Identification flow

The present identification method combines the previous method (Takewaki and Nakamura 2000, 2005) with the high-pass filtering and the ARX modeling. First of all, the number of orders of the ARX model and the cut-off frequency for the high-pass filtering in time domain are needed to determine. A detailed explanation of the determination of these parameters is shown later. When the number of orders of the ARX model and the cut-off frequency are given, the outline of the flow for story stiffness identification is summarized in Fig. 4. In this flowchart, the identification function can be derived by the transfer function using the ARX model after the high-pass filtering is applied to the measured raw data. To eliminate noise in a low frequency range, let us introduce the following high-pass filter function.

$$H(\omega) = \begin{cases} 0 & (0 < \omega < \omega_c) \\ 1 & (\omega_c \leq \omega \leq \omega_{\max}) \end{cases} \quad (34)$$

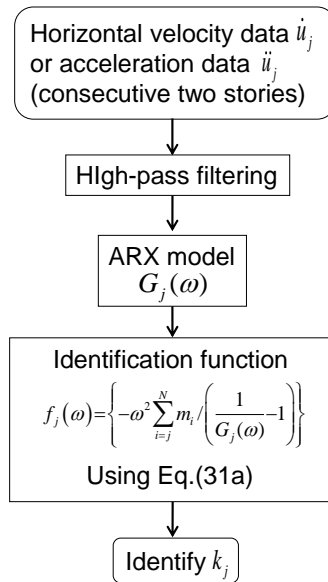


Fig.4 Identification procedure

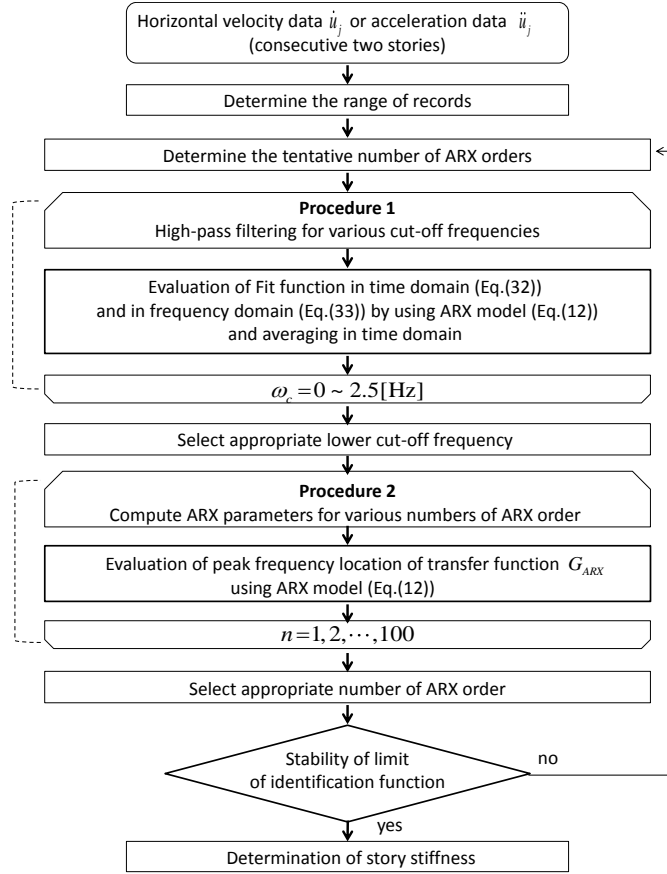


Fig. 5(a) Averaging and filtering of recorded data and overall identification flow

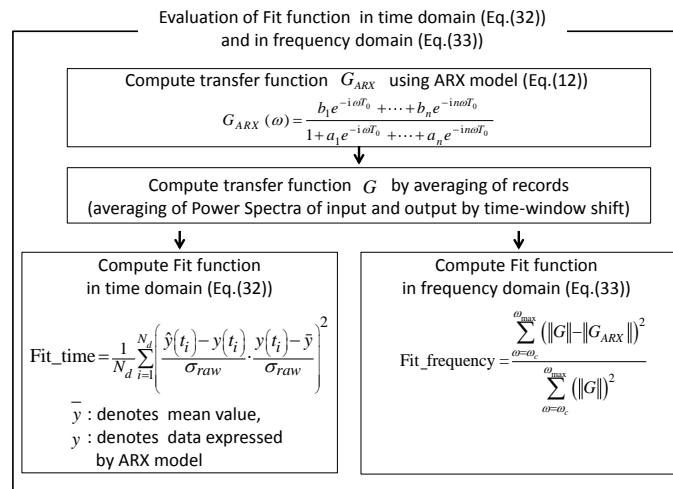


Fig. 5(b) Detailed flow for Procedure 1

It should also be remarked that Eq. (31a) is used in the evaluation of the identification function

in Fig. 4 for reliable evaluation of story stiffnesses.

The flowchart in Fig. 5(a) illustrates a more detailed explanation on the determination of the number of orders of the ARX model and the cut-off frequency for the high-pass filtering in time domain. These procedures are composed of two phases. Before starting these procedures, it is needed to select the range of records for system identification in time domain from the measured raw data.

First, Procedure 1 is the process for determining the cut-off frequency  $\omega_c$  of the high-pass filtering, i.e. high-pass filtering using a tentative number of ARX orders. Second, Procedure 2 is the process for determining the number of orders of the ARX model. In Procedure 1, the fitness functions defined in Eqs. (32) and (33) are evaluated in time and frequency domains, respectively. A detailed flowchart for the evaluation of these fitness functions is illustrated in the flowchart in Fig. 5(b). The comparison of the transfer functions (one from the averaged procedure and the other from the high-pass filtering) is a key procedure for stable implementation of the proposed identification method. In Procedure 2, the stability of the location of the peak frequency of transfer function  $G_{ARX}$  is evaluated. The limit value at  $\omega=0$  of the identification function is affected by the location of the first peak frequency of transfer function  $G_{ARX}$  corresponding to the numbers of the ARX order. The stability of the location of the peak frequency of transfer function  $G_{ARX}$  is directly related to the reliability of the ARX model.

Once the number of orders of the ARX model and the cut-off frequency are determined, the story stiffnesses can be derived from the stable limit value of the identification function. When it is difficult to evaluate the limit value of the identification functions, the number of ARX orders chosen in Procedure 1 needs to be updated.

## 7. Application of story-wise stiffness identification method to actual ambient vibration data

Actual micro-tremor observations were conducted in an experimental real-size building at the Uji campus of Kyoto University. The building overview is shown in Fig. 6 and the installation situation of velocity meters is illustrated in Fig. 7. The frame dimension and its shear building model are shown in Fig. 8. The locations of velocity meters for three patterns of identification are presented in Fig. 9. The floor masses are shown in Table 1. The measurement location, identified stories and measurement durations are shown in Table 2. Pattern A is aimed at identifying the story stiffnesses of the first and second stories and pattern B the fourth and fifth stories. On the other hand, pattern C is set for identifying the third story stiffness.

In addition to story-wise micro-tremor observations shown in Table 2, (i) static frame response analysis, (ii) forced vibration tests (vibration source is on the roof) and (iii) another micro-tremor observation on the ground and roof were performed. The static response analysis was performed by applying horizontal static loads on a plane frame model and a three-dimensional frame model. The member cross-section list has been taken from the previous work (Le and Tamura 2009) and the floor masses have been computed based on the measurement of size. The natural frequencies and story stiffnesses estimated by these methods (i)-(iii) are used later for comparison.

Fig. 10 illustrates some examples of recorded data (ground, third floor, fourth floor and roof) in the short-span direction in Pattern C. Figs. 11(a) and (b) show the transfer functions between the base and roof in the short-span and long-span directions, respectively. These transfer functions

have been plotted for investigating the natural frequencies of this building. The mean values of peak-amplitude frequencies are shown in Tables 3 and 4 as the natural frequencies identified from the ambient vibration data.

Fig. 12 presents the comparison between the original time-domain data and those after high-pass filtering. It can be observed that a good filtering has been conducted.

Fig. 13(a) illustrates the limit value at  $\omega = 0$  of the real part of the identification function, Eq.(31a), and Fig. 13(b) shows the corresponding time-domain and frequency-domain fitness functions called 'Fit' (Eq.(32) and Eq.(33)) for the first story with respect to the cut-off frequency in the short-span direction (Pattern A). The number 30 of ARX order was chosen temporarily. The cut-off frequency has been varied in the range of 0~2.5[Hz]. The maximum frequency corresponds approximately to the fundamental natural frequency of the object building frame. It can be observed that a stable property exists in the range of 0.6~1.8[Hz] from both viewpoints of stiffness identification and fitness evaluation. The cut-off frequency 1[Hz] has then been chosen judging from the stable time-domain and frequency-domain fitting.

Fig. 14 illustrates the limit value at  $\omega = 0$  of the real part of the identification function, Eq. (31a), for the first story with respect to the number of orders of the ARX model in the long-span direction (Pattern A). As shown in Eq. (31a), the expression of the stiffness in terms of the ARX parameters (Eqs. (14)-(16)) supports the stability of stiffness identification. It can be observed from Fig.14 that a stable property exists in the range of the number of ARX model larger than 20. Fig. 15 shows the peak frequency of the transfer function for the first story using the ARX model with respect to the number of orders of the ARX model in the long-span direction (Pattern A). It can be observed from Fig. 15 that a similar stable property exists in the range of the number of ARX model larger than 20. As a result, the numbers 40 to 60 of the ARX orders has been chosen in this case. The mean value for the numbers 40 to 60 of the ARX orders was adopted as the identified value of the stiffness.

Figs. 13, 14 and 15 clearly show the stability of identification using the ARX model.

Fig. 16 presents the real part of the identification functions in the short-span direction (Pattern A) using the original recorded data, the data using the ARX model (without filtering) and the data using the ARX model (with filtering). It can be found that the filtering is absolutely necessary for reliable identification in addition to the application of the ARX model.



Fig.6 Five-story steel building



Fig.7 Installation of velocity meter

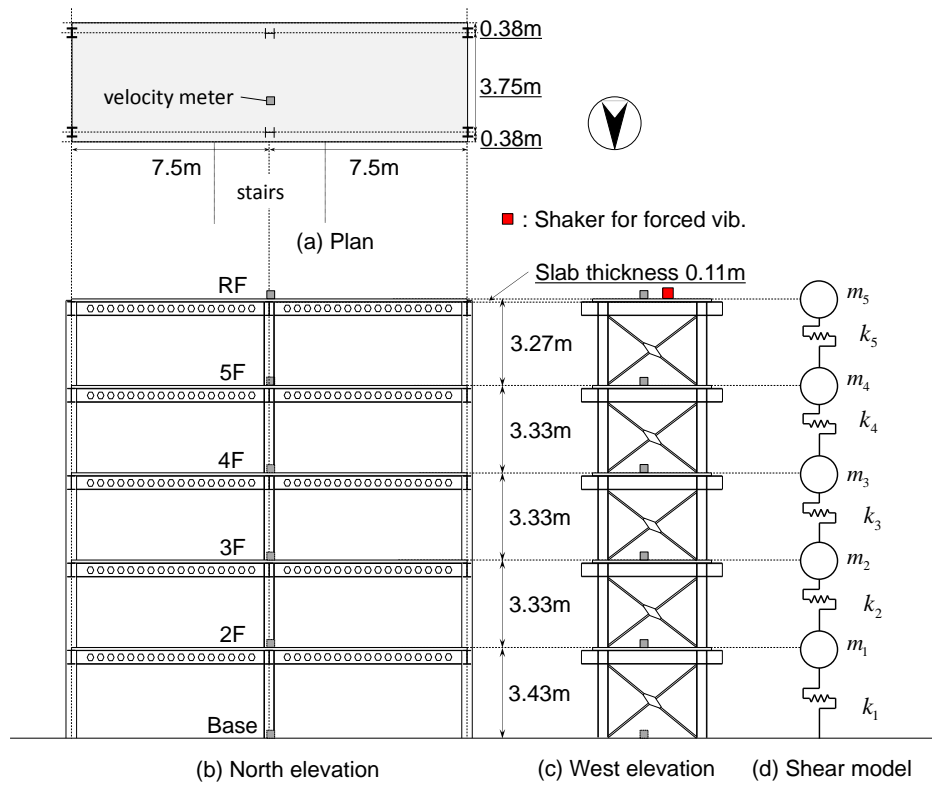


Fig.8 Frame dimension and its shear building model

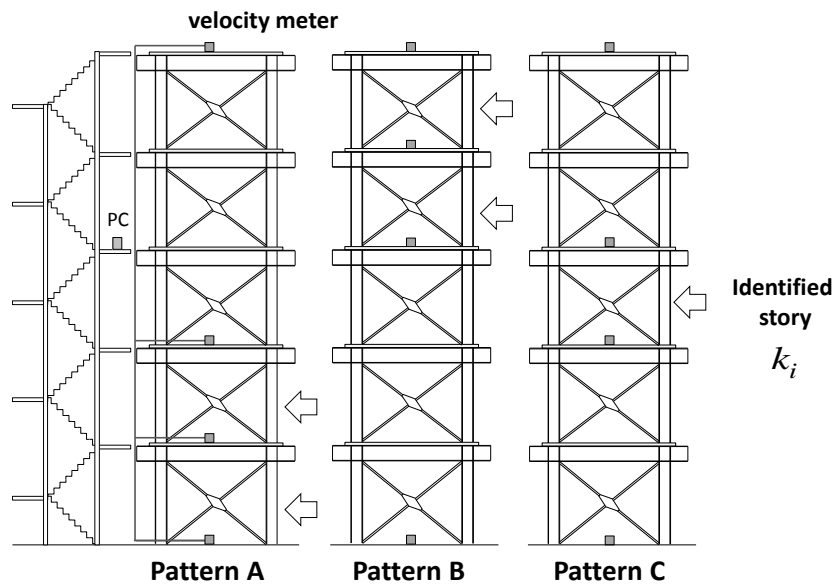


Fig. 9 Location of velocity meters for three patterns of identification

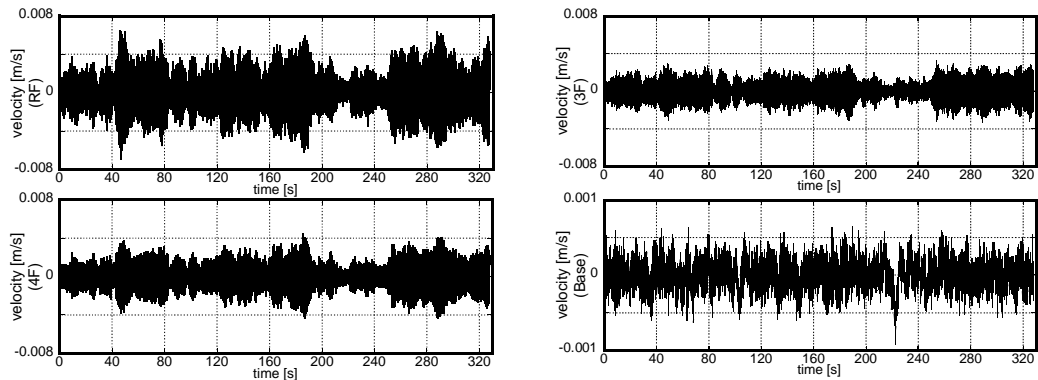
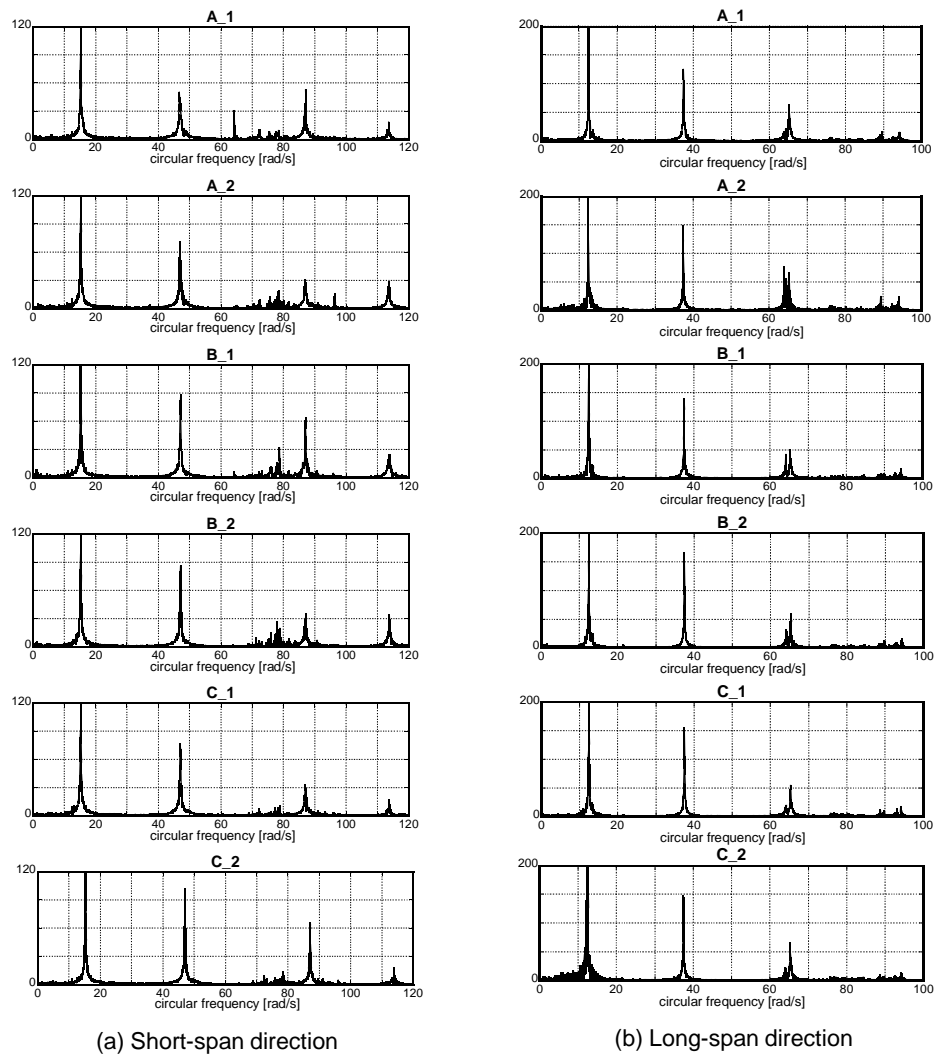


Fig. 10 Examples of recorded data (ground level, 3rd floor, 4th floor and roof)



(a) Short-span direction

(b) Long-span direction

Fig. 11 Transfer functions between the base and roof (Roof/Base)

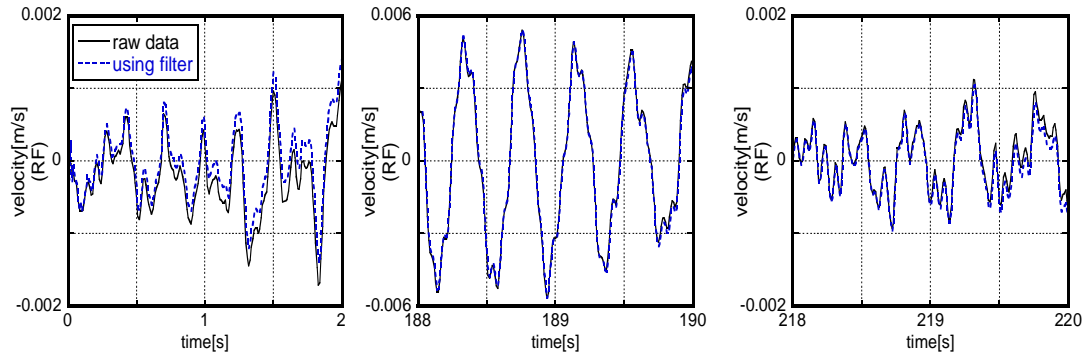
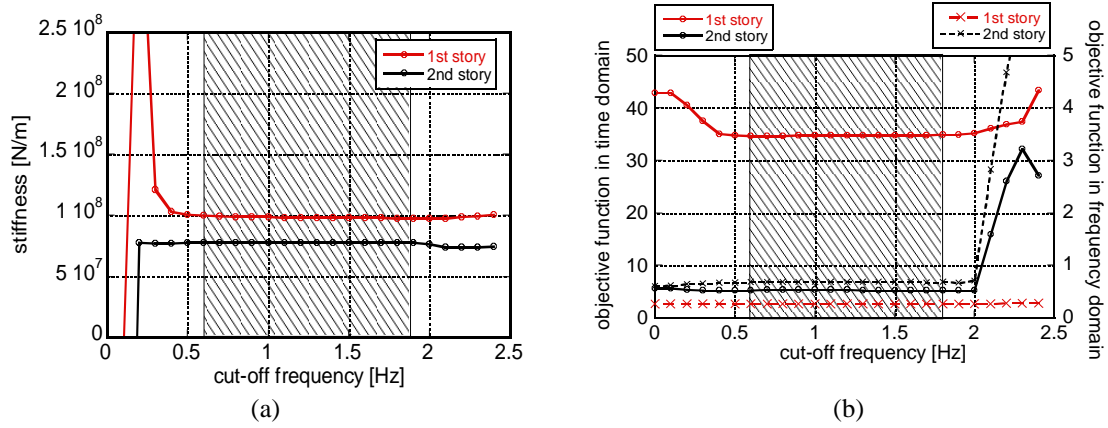
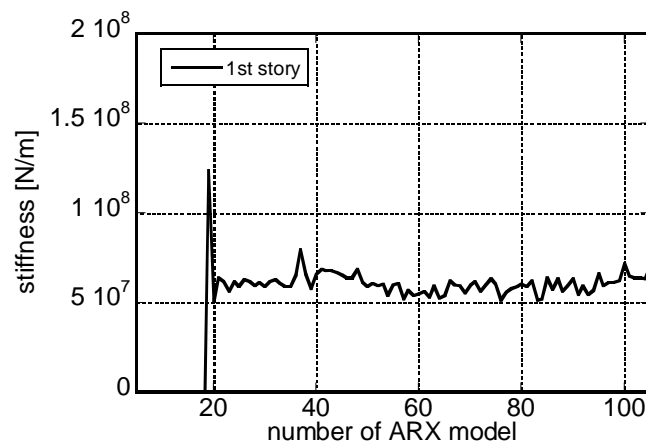


Fig. 12 Comparison between the original data and those after high-pass filtering

Fig. 13 Limit value at  $\omega = 0$  of real part of identification function and fitness for the first story with respect to the cut-off frequency  $\omega_c$  in the short-span direction (Pattern A)Fig. 14 Limit value at  $\omega=0$  of real part of identification function for the first story with respect to the number of ARX orders in the long-span direction (Pattern A)



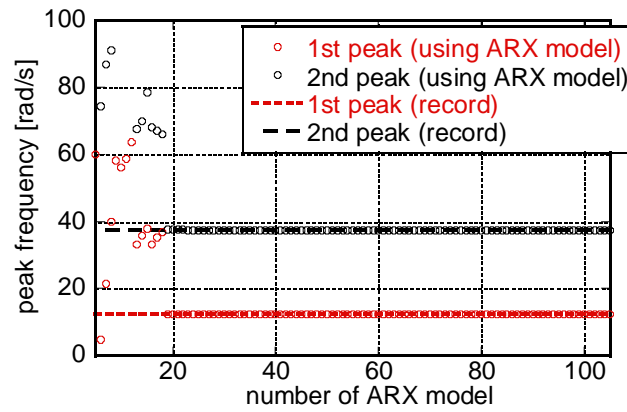


Fig. 15 Peak frequency of the transfer function using ARX model with respect to the number of ARX orders in the long-span direction (Pattern A)

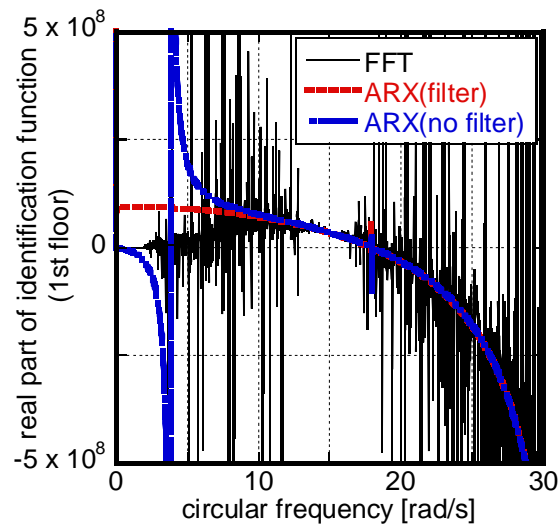


Fig. 16 Real part of identification function in the short-span direction (Pattern A) using the original recorded data, the data in terms of the ARX model (without high-pass filtering) and the data in terms of the ARX model (with high-pass filtering)

Table 1 Floor masses

	floor mass [ $\times 10^3$ kg]
$m_5$	26.6
$m_4$	27.6
$m_3$	27.6
$m_2$	28.2
$m_1$	28.7

Table 2 Measurement location, identified stories and measurement duration

Pattern	Measurement location	Identified story	Measurement duration
A_1	GL, 2F, 3F, RF	1, 2	5min
A_2			10min
B_1	GL, 4F, 5F, RF	4, 5	5min
B_2			10min
C_1	GL, 3F, 4F, RF	3	5min
C_2			10min

Table 3 Summary of identification (Short-span direction)

		Preliminary static analysis	Forced vib. test	Ambient vib. data (Roof/base)	Identified value (Eq.(8))
stiffness ( $\times 10^4$ [kN/m])	1st story	10.82	-	-	10.07
	2nd story	9.83	-	-	8.403
	3rd story	9.56	-	-	7.656
	4th story	9.23	-	-	6.041
	5th story	8.49	-	-	5.024
natural circular frequency [rad/s]	1st	17.19	15.07	15.19	15.59
	2nd	48.75	46.83	46.89	41.39
	3rd	76.16	72.09	76.02	64.97
	4th	97.44	86.50	86.93	82.70
	5th	111.77	113.21	113.72	99.88
natural frequency [Hz]	1st	2.74	2.40	2.42	2.48
	2nd	7.76	7.46	7.46	6.59
	3rd	12.13	11.48	12.10	10.34
	4th	15.52	13.77	13.84	13.16
	5th	17.80	18.03	18.10	15.90

Table 4 Summary of identification (Long-span direction)

		Preliminary static analysis	Forced vib. test	Ambient vib. data (Roof/base)	Identified value (Eq.(8))
stiffness $\times 10^4$ [kN/m]	1st story	5.12	-	-	6.038
	2nd story	4.55	-	-	5.402
	3rd story	4.51	-	-	4.912
	4th story	4.47	-	-	4.612
	5th story	4.44	-	-	4.424
natural circular frequency [rad/s]	1st	11.81	12.37	12.19	12.60
	2nd	34.04	37.24	37.47	35.33
	3rd	53.32	65.12	65.05	55.35
	4th	67.95	93.82		70.77
	5th	77.24	118.38		80.95
natural circular frequency [Hz]	1st	1.88	1.97	1.94	2.01
	2nd	5.42	5.93	5.97	5.62
	3rd	8.49	10.37	10.36	8.81
	4th	10.82	14.94		11.26
	5th	12.30	18.85		12.88

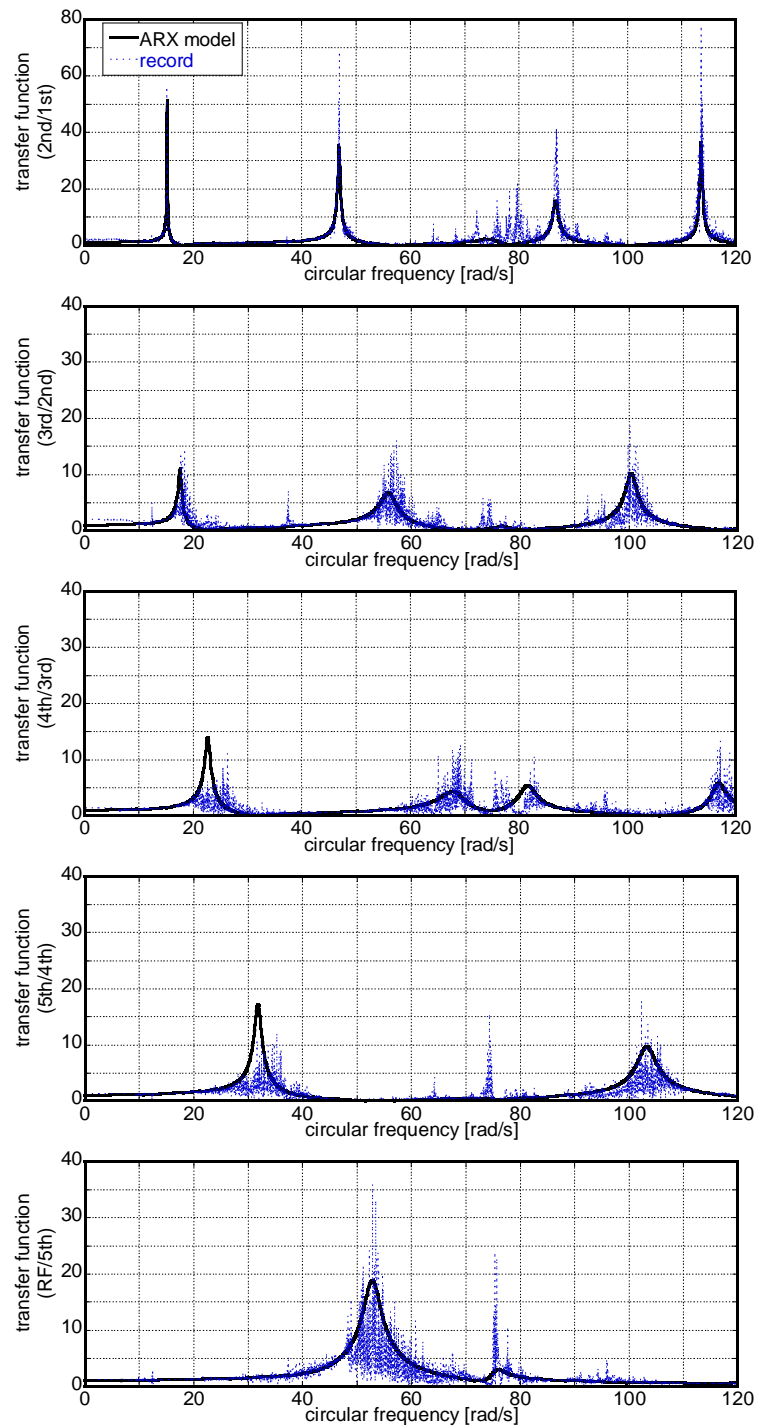


Fig. 17 Transfer function between the upper and lower floors of respective stories in short-span direction: comparison of function using FFT of original data and that using ARX model

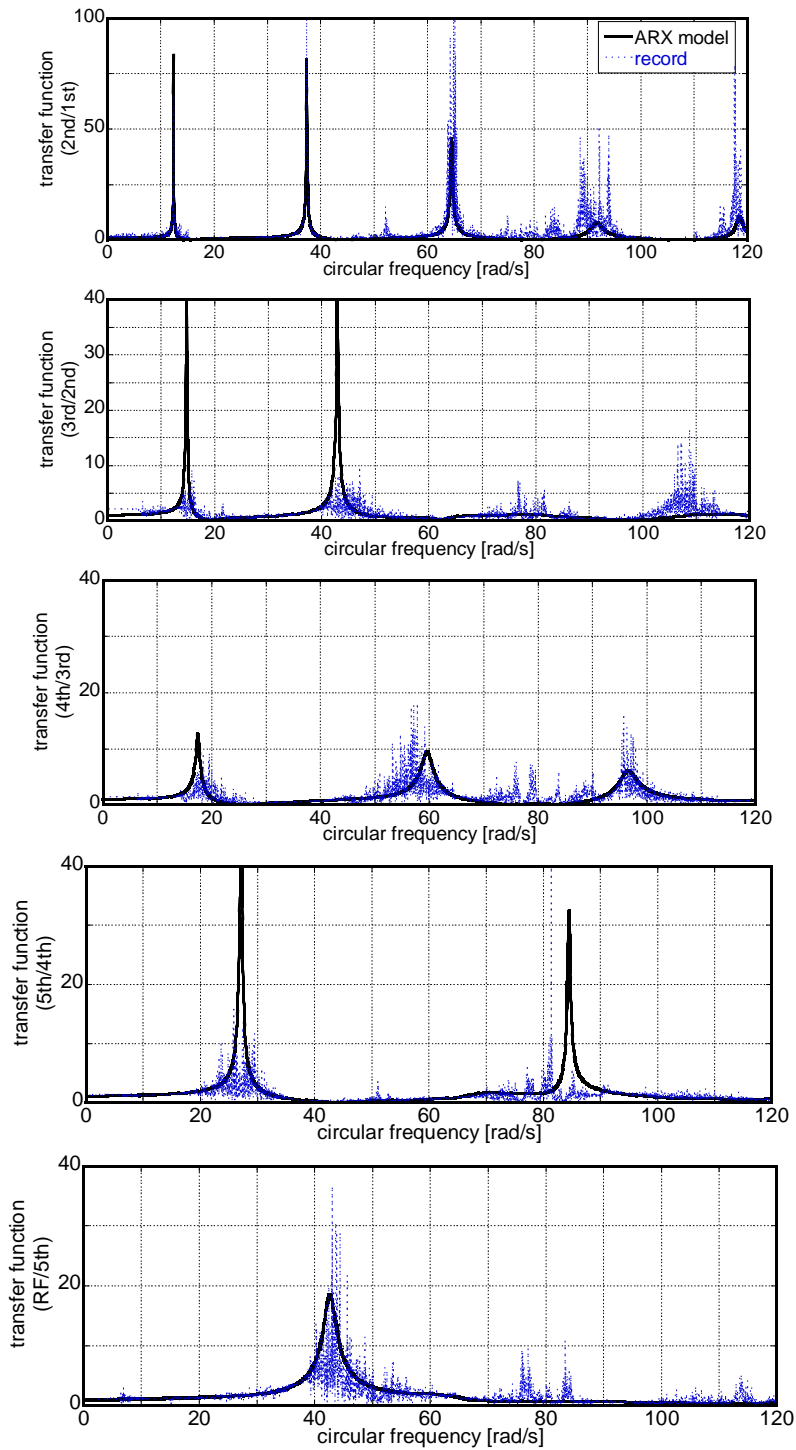


Fig. 18 Transfer function between the upper and lower floors of respective stories in long-span direction: comparison of function using FFT of original data and that using ARX model

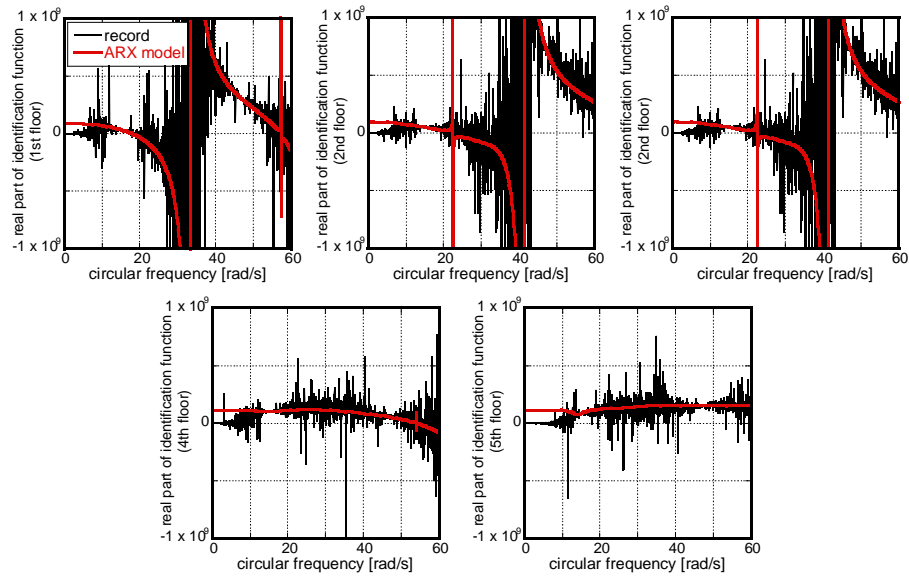


Fig. 19 Real part of identification function in short-span direction: comparison of function using FFT of original data and that using ARX model

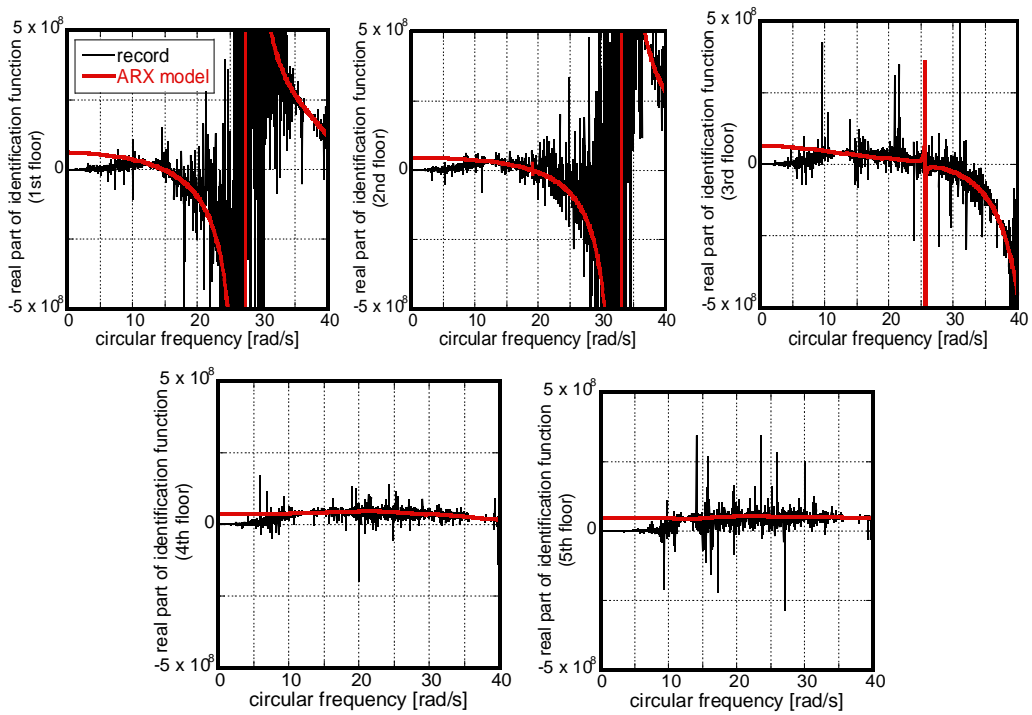


Fig. 20 Real part of identification function in long-span direction: comparison of function using FFT of original data and that using ARX model

Fig. 17 illustrates the transfer functions, Eq.(11), between the upper and lower floors of respective stories in the short-span direction using the data after application of the filtering and the ARX model and the data after application of the filtering. It can be observed that the ARX model is effective for the reliable estimation of transfer functions. Fig.18 shows the transfer function between the upper and lower floors of respective stories in the long-span direction. This figure also supports the effectiveness of the ARX model.

Fig. 19 presents the real part of the identification functions in the short-span direction using the transfer functions shown in Fig. 17. Fig. 20 illustrates the real part of the identification functions in the long-span direction using the transfer functions shown in Fig.18. The limit value at  $\omega = 0$  represents the story stiffness. It can be understood that the ARX model is inevitable for reliable and stable identification of story stiffness in the proposed method.

Table 3 summarizes the comparison in the short-span direction among the preliminary static response analysis using a frame model, the forced vibration test and the ambient vibration data analysis using micro-tremor at the base and roof. On the other hand, Table 4 summarizes the comparison in the long-span direction among the preliminary static response analysis using a frame model, the forced vibration test and the ambient vibration data analysis using micro-tremor at the base and roof. It can be observed that, while the preliminary static response analysis in the short-span direction provides a slightly stiffer result compared with the forced vibration test and the ambient vibration data analysis, the preliminary static response analysis in the long-span direction provides a slightly flexible result compared with the forced vibration test and the ambient vibration data analysis. It should be remarked that the natural frequencies (especially the lowest one) of the model identified by the proposed method coincide fairly well with those by the forced vibration tests (vibration source is on the roof) and another micro-tremor observation rather than those by the preliminary static response analysis. It can be concluded from Tables 3 and 4 that the present system identification method using ambient vibration data is reliable and practical.

## 8. Conclusions

A previously proposed story-wise stiffness identification method for a shear building structure is applied to the case where the shear building is subjected to micro-tremor. While earthquake ground motions and the building responses to such inputs are necessary in the previous method, it is shown that micro-tremors can be used for identification within the same framework. This enhances the usability of the previously proposed identification method. The difficulty arising in the limit manipulation at zero frequency in the previous method is overcome by introducing an ARX model, filtering in the frequency range (low cut) and averaging in time domain (sequential time-window shift). The weakness of small SN ratio in the low frequency range is avoided by using the ARX model and introducing new constraints on the ARX parameters. Advantageous features are as follows:

- (1) Micro-tremor can be used as an input for the previously proposed story-wise identification method for shear building models regardless of its small vibration level.
- (2) Filtering in the frequency range (low cut) and averaging in time domain (sequential time-window shift for Fourier transformation and averaging) are necessary for reliable identification for such ambient vibration.
- (3) An ARX model is shown to be useful for reliable and accurate identification. Unstable properties of the identification function have been eliminated.

## Acknowledgements

This research is partly supported by the Grant-in-Aid for Scientific Research (No. 24246095) in Japan. This support is gratefully acknowledged.

## References

- Adachi S. (2009), *Fundamentals of System Identification*, Tokyo Denki University Press (in Japanese).
- Agbabian, M.S., Masri, S.F., Miller, R.K. and Caughey, T.K. (1991), System identification approach to detection of structural changes, *J. Engng. Mech.*, ASCE; **117**(2): 370-390.
- Barroso, L.R. and Rodriguez, R. (2004), Damage detection utilizing the damage index method to a benchmark structure. *J. Engng. Mech.*, ASCE; **130**(2): 142-151.
- Beck, J.L. and Jennings, P.C. (1980), Structural identification using linear models and earthquake records, *Earthquake Engng. Struct. Dyn.*; **8**: 145-160.
- Bernal, D. and Beck, J. (2004), Preface to the Special Issue on Phase I of the IASC- ASCE Structural Health Monitoring Benchmark, *J. Engng. Mech.*, ASCE; **130**(1): 1-2.
- Casciati, F. (ed.) (2002), *Proceedings of 3rd World Conference on Structural Control*. John Wiley & Sons: Como.
- Doebling, S.W., Farrar, C.R., Prime, M.B. and Shevitz, D.W. (1996), *Damage identification and health monitoring of structural and mechanical systems from changes in their vibration characteristics: A literature review*, Los Alamos National Laboratory Report LA-13070-MS.
- Fujino, Y., Nishitani, A. and Mita, A. (2010), *Proceedings of 5th World Conference on Structural Control and Monitoring, (5WCSCM)*. Tokyo.
- Fujita, K., Ikeda, A., Shirono, M. and Takewaki, I. (2013), System identification of high-rise buildings using shear-bending model and ARX model: Experimental investigation, *Proc. of ICEAS13 in ASEM13*, September 8-12, Jeju, Korea, pp2803-2815.
- Ghanem, R. and Shinozuka, M. (1995), Structural-system identification I: Theory, *J. Engng. Mech.*, ASCE; **121**(2), 255-264.
- Hart, G.C. and Yao, J.T.P. (1977), System identification in structural dynamics, *J. Engng. Mech. Div.*, ASCE; **103**(EM6): 1089-1104.
- Hernandez-Garcia, M.R., Masri, S.F., Ghanem, R., Figueiredo, E. and Farrar, C.R. (2010), An experimental investigation of change detection in uncertain chain-like systems. *J. Sound Vib.*; **329**(12), 2395-2409.
- Hernandez-Garcia, M., Masri, S.F., Ghanem, R., Figueiredo, E. and Farrar, R.A. (2010), A structural decomposition approach for detecting, locating, and quantifying nonlinearities in chain-like systems. *Struct. Control Health Monitor.*, **17**, 761-777.
- Hjelmstad, K.D., Banan, M.R. and Banan, M.R. (1995), On building finite element models of structures from modal response, *Earthq. Eng. Struct. Dyn.*, **24**, 53-67.
- Hjelmstad K.D. (1996), On the uniqueness of modal parameter estimation, *J. Sound Vib.*; **192**(2), 581-598.
- Hoshiya, M. and Saito, E. (1984), Structural identification by extended Kalman filter, *J. Eng. Mech.*, ASCE; **110**(12), 1757-1770.
- Housner, G.W., Masri, S.F. and Chassiakos, A.G., (1994), *Proceedings of 1st World Conference on Structural Control*. IASC: Los Angeles, CA.
- Housner G.W., Bergman, L., Caughey, T., Chassiakos, A., Claus, R., Masri, S., Skelton, R., Soong, T., Spencer, B. and Yao, J. (1997), "Special issue, Structural control: past, present, and future", *J. Eng. Mech.*, ASCE, **123**(9): 897-971.
- Ji, X., Fenves, G.L.; Kajiwar, K. and Nakashima, M. (2011), "Seismic damage detection of a full-scale shaking table test structure", *J. Struct. Eng.* ASCE, **137**(1), 14-21.
- Johnson E. and Smyth A. (2006), *Proceedings of 4th World Conference on Structural Control and*

- Monitoring, (4WCSCM)*. IASC: San Diego, CA.
- Johnson, E.A., Lam, H.F., Katafygiotis, L.S., Beck, J.L. (2004), Phase I IASC-ASCE Structural Health Monitoring Benchmark Problem using Simulated Data. *ASCE J. Eng. Mech.*, **130**(1), 3-15.
- Kobori, T., Inoue, Y., Seto, K., Iemura, H. and Nishitani, A. (1998), *Proceedings of 2nd World Conference on Structural Control*. John Wiley & Sons: Kyoto.
- Koh, C.G., See, L.M and Balendra, T. (1991), Estimation of structural parameters in time domain: a substructure approach, *Earthq. Eng. Struct. Dyn.*; **20**: 787-801.
- Kozin, F. and Natke, H.G. (1986). System identification techniques, *Struct. Safety*, **3**, 269-316.
- Kuwabara, M, Yoshitomi, S and Takewaki, I. (2013). A new approach to system identification and damage detection of high-rise buildings, *Struct. Control Health Monitor.*, **20**, 703-727.
- Le, T.H. and Tamura, Y. (2009). Modal identification of ambient vibration structure using frequency domain decomposition and wavelet transform, *Proceeding of the Seventh Asia-Pacific Conference on Wind Engineering*, November 8-12, 2009, Taipei, Taiwan.
- Lus, H., Betti, R., Yu, J. and De Angelis, M. (2004), Investigation of a system identification methodology in the context of the ASCE benchmark problem, *J. Eng. Mech.*, ASCE; **130**(1), 71-84.
- Maeda, T., Yoshitomi, S. and Takewaki, I. (2011), Stiffness-damping identification of buildings using limited earthquake records and ARX model, *J. Struct. Construction Eng.*, Architectural Inst. of Japan; **666**: 1415-1423 (in Japanese).
- Masri, S.F., Nakamura M., Chassiakos, A.G. and Caughey, T.K. (1996), A neural network approach to the detection of changes in structural parameters, *J. Eng. Mech.*, ASCE; **122**(4), 350-360.
- Mendel, J.M. (1995), *Lessons in Estimation Theory for Signal Processing, Communications, and Control*, 2nd Edition, Prentice Hall.
- Minami, Y., Yoshitomi, S. and Takewaki, I. (2013), System identification of super high-rise buildings using limited vibration data during the 2011 Tohoku (Japan) earthquake, *Struct. Control Health Monitor.*, **20**, 1317-1338.
- Nagarajaiah, S. and Basu, B. (2009), Output only modal identification and structural damage detection using time frequency & wavelet techniques, *Earthq. Eng.Eng. Vib.*; **8**(4), 583-605.
- Safak, E. (1989), Adaptive Modeling, Identification, and control of dynamic structural systems. I: Theory, *J. Eng. Mech.*, ASCE; **115**(11), 2386-2405.
- Shinozuka, M. and Ghanem, R. (1995), "Structural-system identification II: Experimental verification", *J. Eng. Mech.*, ASCE; **121**(2), 265-273.
- Takewaki, I. and Nakamura, M. (2000), "Stiffness-damping simultaneous identification using limited earthquake records", *Earthq. Eng. Struct. Dyn.*, **29**(8), 1219-1238.
- Takewaki, I. and Nakamura, M. (2005), "Stiffness-damping simultaneous identification under limited observation", *J. Eng. Mech.*, ASCE; **131**(10), 1027-1035.
- Takewaki, I. and Nakamura, M. (2009), "Temporal variation of modal properties of a base-isolated building during an earthquake", *J. Zhejiang University-SCIENCE A*; **11**(1), 1-8.
- Udwadia, F.E., Sharma, D.K and Shah, P.C. (1978), "Uniqueness of damping and stiffness distributions in the identification of soil and structural systems", *J. Applied Mech.*, ASME; **45**: 181-187.
- Xing, Z. and Mita, A. (2012), "A substructure approach to local damage detection of shear structure", *Struct. Control Health Monitor.*, **19**(2), 309-318.
- Yao, J.T.P. and Natke, H.G. (1994), Damage detection and reliability evaluation of existing structures, *Struct. Safety*; **15**: 3-16.
- Zhang D.Y. and Johnson, E.A. (2012), Substructure Identification for Shear Structures: Cross Power Spectral Density Method, *Smart Mater. Struct.*, **21**(5), 055006.
- Zhang D.Y. and Johnson, E.A. (2013a). Substructure identification for shear structures I: Substructure identification method, *Struct. Control Health Monitor.*, **20**(5), 804-820.
- Zhang D.Y. and Johnson, E.A. (2013b), "Substructure identification for shear structures with nonstationary structural responses", *J. Eng. Mech.*, ASCE, **139**(12), 1769-1779.



## Appendix 1 ARX model (Adachi 2009)

Let  $k$  denote a discrete time step. When the output, the input and white noise are denoted by  $y(\cdot)$ ,  $u(\cdot)$  and  $w(\cdot)$ , the ARX model is described by

$$y(k) + a_1 y(k-1) + \dots + a_{n_a} y(k-n_a) = b_1 u(k-1) + \dots + b_{n_b} u(k-n_b) + w(k) \quad (\text{A1})$$

The transfer function can be expressed in terms of the shift operator  $q$ .

$$G(q) = B(q)/A(q) \quad (\text{A2})$$

where

$$A(q) = 1 + a_1 q^{-1} + \dots + a_{n_a} q^{-n_a} \quad (\text{A3})$$

$$B(q) = b_1 q^{-1} + \dots + b_{n_b} q^{-n_b} \quad (\text{A4})$$

The relation between the Z transformation and the Fourier transformation is given by Eq.(A5) and the transfer function in terms of the variable  $q$  in Eq.(A2) can be expressed as the transfer function in terms of the variable  $\omega$  (circular frequency). In Eq.(A5),  $T_0$  denotes the sampling period.

$$q = e^{i\omega T_0} \quad (\text{A5})$$

$$G(\omega) = \frac{b_1 e^{-i\omega T_0} + \dots + b_{n_b} e^{-in_b \omega T_0}}{1 + a_1 e^{-i\omega T_0} + \dots + a_{n_a} e^{-in_a \omega T_0}} \quad (\text{A6})$$

## Appendix 2 Prediction error in ARX model

Define the parameter vector  $\theta$  and the data vector  $\phi(k)$  by Eqs.(A7) and (A8), respectively. The prediction of the output at time  $k$  from the input-output data until time  $(k-1)$  can be expressed by Eq.(A9).

$$\theta = \{a_1 \quad \dots \quad a_{n_a} \quad b_1 \quad \dots \quad b_{n_b}\}^T \quad (\text{A7})$$

$$\phi(k) = \{-y(k-1) \quad \dots \quad -y(k-n_a) \quad u(k-1) \quad \dots \quad u(k-n_b)\}^T \quad (\text{A8})$$

$$\hat{y}(k; \theta) = \theta^T \phi(k) \quad (\text{A9})$$

Using Eq.(A9), the prediction error in the ARX model can be described by

$$\varepsilon(k, \theta) = y(k) - \hat{y}(k; \theta) = y(k) - \theta^T \phi(k) \quad (\text{A10})$$

### Appendix 3 Least-mean-square estimate of parameter vector

Introduce the objective function by Eq.(A11) for predicting the parameter vector  $\boldsymbol{\theta}$ . Then the least-squares method can be applied to the parameter prediction problem.

$$J_N(\boldsymbol{\theta}) = \frac{1}{N_d} \sum_{k=1}^{N_d} \varepsilon^2(k; \boldsymbol{\theta}) \quad (\text{A11})$$

In this case, the prediction problem of  $\boldsymbol{\theta}$  can be reduced to the following simultaneous equations.

$$\mathbf{R}\boldsymbol{\theta} = \mathbf{f} \quad (\text{A12})$$

where

$$\mathbf{R} = \frac{1}{N_d} \boldsymbol{\Phi} \boldsymbol{\Phi}^T \quad \left( \boldsymbol{\Phi} = [\boldsymbol{\varphi}(1) \quad \boldsymbol{\varphi}(2) \quad \cdots \quad \boldsymbol{\varphi}(N_d)]^T \right) \quad (\text{A13})$$

$$\mathbf{f} = \frac{1}{N_d} \boldsymbol{\Phi}^T \mathbf{y} \quad \left( \mathbf{y} = \{y(1) \quad y(2) \quad \cdots \quad y(N_d)\}^T \right) \quad (\text{A14})$$

The least-square estimation of the unknown parameters based on the  $N_d$ -pair input-output measured data may then be expressed by

$$\hat{\boldsymbol{\theta}} = \mathbf{R}^{-1} \mathbf{f} \quad (\text{A15})$$